

**Manuscript version: Author's Accepted Manuscript**

The version presented in WRAP is the author's accepted manuscript and may differ from the published version or Version of Record.

**Persistent WRAP URL:**

<http://wrap.warwick.ac.uk/133148>

**How to cite:**

Please refer to published version for the most recent bibliographic citation information. If a published version is known of, the repository item page linked to above, will contain details on accessing it.

**Copyright and reuse:**

The Warwick Research Archive Portal (WRAP) makes this work by researchers of the University of Warwick available open access under the following conditions.

Copyright © and all moral rights to the version of the paper presented here belong to the individual author(s) and/or other copyright owners. To the extent reasonable and practicable the material made available in WRAP has been checked for eligibility before being made available.

Copies of full items can be used for personal research or study, educational, or not-for-profit purposes without prior permission or charge. Provided that the authors, title and full bibliographic details are credited, a hyperlink and/or URL is given for the original metadata page and the content is not changed in any way.

**Publisher's statement:**

Please refer to the repository item page, publisher's statement section, for further information.

For more information, please contact the WRAP Team at: [wrap@warwick.ac.uk](mailto:wrap@warwick.ac.uk).

# Ir $5d$ -band Derived Superconductivity in $\text{LaIr}_3$

A Bhattacharyya<sup>1\*</sup>, D T Adroja<sup>2,3†</sup>, P K Biswas<sup>2</sup>, Y J Sato<sup>4,5</sup>,  
M R Lees<sup>6</sup>, D Aoki<sup>5</sup> and A D Hillier<sup>2</sup>

<sup>1</sup> Department of Physics, Ramakrishna Mission Vivekananda Educational and Research Institute, Belur Math, Howrah 711202, West Bengal, India

<sup>2</sup> ISIS Facility, Rutherford Appleton Laboratory, Chilton, Didcot Oxon, OX11 0QX, United Kingdom

<sup>3</sup> Highly Correlated Matter Research Group, Physics Department, University of Johannesburg, PO Box 524, Auckland Park 2006, South Africa

<sup>4</sup> Graduate School of Engineering, Tohoku University, Sendai 980-8577, Japan

<sup>5</sup> Institute for Materials Research, Tohoku University, Oarai, Ibaraki 311-1313, Japan

<sup>6</sup> Department of Physics, University of Warwick, Coventry CV4 7AL, United Kingdom

E-mail: \*[amitava.bhattacharyya@rkmvu.ac.in](mailto:amitava.bhattacharyya@rkmvu.ac.in),

†[devashibhai.adroja@stfc.ac.uk](mailto:devashibhai.adroja@stfc.ac.uk)

## Abstract.

The superconducting properties of rhombohedral  $\text{LaIr}_3$  were examined using susceptibility, resistivity, heat capacity, and zero-field (ZF) and transverse-field (TF) muon spin relaxation and rotation ( $\mu\text{SR}$ ) measurements. The susceptibility and resistivity measurements confirm a superconducting transition below  $T_C = 2.5(1)$  K. Two successive transitions are observed in the heat capacity data, one at  $T_C = 2.5$  K and a second at 1.2 K below  $T_C$ . The heat capacity jump is  $\Delta C/\gamma T_C \sim 1.0$  which is lower than 1.43 expected for Bardeen-Cooper-Schrieffer (BCS) weak-coupling limit. Transverse-field- $\mu\text{SR}$  measurements reveal a fully gapped  $s$ -wave superconductivity with  $2\Delta(0)/k_B T_C = 3.31(8)$ , which is small compared to BCS value of 3.56, suggesting weak-coupling superconductivity. The magnetic penetration depth,  $\lambda_L(0)$ , estimated from TF- $\mu\text{SR}$  gives  $\lambda_L(0) = 386(3)$  nm, a superconducting carrier density  $n_s = 2.9(1) \times 10^{27}$  carriers  $m^{-3}$  and a carrier effective-mass enhancement factor  $m^* = 1.53(1)m_e$ . ZF- $\mu\text{SR}$  data show no evidence for any spontaneous magnetic fields below  $T_C$ , which demonstrates that time-reversal symmetry is preserved in the superconducting state of  $\text{LaIr}_3$ .

**Keywords.** Superconducting gap structure;  $d$ -band superconductivity; Muon spin rotation and relaxation spectroscopy

PACS numbers: 71.20.Be, 75.10.Lp, 76.75.+i

## 1. Introduction

The search for unconventional superconductivity in 5d transition metal-based compounds is one of the most fascinating and significant problems in condensed matter physics [1, 2, 3, 4]. Due to the presence of strong spin-orbit (SO) coupling effects, the 5d transition metal compounds have been extensively studied to investigate the correlation between strong SO coupling and unconventional superconductivity [5, 6]. Similar energy scales for the comparatively weak electronic correlations (0.5 to 3 eV), crystal-field effects (1 to 5 eV) and strong relativistic SO coupling effects (0.1 to 1 eV) provide an opportunity to investigate the science emerging from competing orbital, spin, charge, and lattice degrees of freedom [7, 8]. For example, pressure-induced superconductivity in 1T-TaS<sub>2</sub> [9], in noncentrosymmetric CePt<sub>3</sub>Si [10], and in the geometrically frustrated pyrochlore oxides Cd<sub>2</sub>Re<sub>2</sub>O<sub>7</sub> [11] and KOs<sub>2</sub>O<sub>6</sub> [12]. In iridium-containing compounds, superconductivity has been reported in materials such as IrSe<sub>2</sub>, Cu<sub>1-x</sub>Zn<sub>x</sub>Ir<sub>2</sub>S<sub>4</sub>, CeIrSi<sub>3</sub>, ScIrP, LaIrP and LaIrAs, and in the ternary ThCr<sub>2</sub>Si<sub>2</sub>-type compounds BaIr<sub>2</sub>P<sub>2</sub> and SrIr<sub>2</sub>As<sub>2</sub> [13, 14, 15, 16, 17, 18]. In the case of the rare-earth Ir based superconductors, their electronic characteristics are anticipated to arise principally from the rare-earths, rather than the Ir. Nevertheless, there are a few materials such as CaIr<sub>2</sub> [19], IrGe [20], and Mg<sub>10</sub>Ir<sub>19</sub>B<sub>16</sub> [21], where the superconductivity emerges from the Ir 5d states. Now, with the discovery of LaIr<sub>3</sub>, there is a simple La-Ir superconductor with strong spin-orbit-coupling whose characteristics are controlled by the Ir 5d bands at the Fermi surface.

Recently, Haldolaarachchige *et al.* [22] reported that LaIr<sub>3</sub> shows superconductivity with a  $T_C$  between 2.45 and 3.3 K and  $\mu H_{c2}(0) = 38.4$  kOe, where the Fermi surface is governed by the Ir 5d bands that are heavily influenced by spin-orbit coupling and there is no strong contribution from the La-orbitals near  $E_F$ . LaIr<sub>3</sub> is, therefore, one of the few superconductors where 5d bands play a principal role in the appearance of superconductivity. Furthermore, a three-dimensional metallic character is seen from the band structure calculations; many bands with large dispersion cross  $E_F$  [22]. LaIr<sub>3</sub> forms with a rhombohedral crystal structure with the space group  $R\bar{3}m$  (166,  $D_{3d}^5$ ). There are two crystallographically inequivalent La sites and three Ir sites [22]. To examine the role the lanthanide elements and the spin-orbit coupling effects arising from the Ir 5d bands play in determining the superconducting properties, the study of other rhombohedral  $R\text{Ir}_3$  materials ( $R$  is a lanthanide with 4f electrons) [23, 24] will be important. In particular, compounds with partly filled 4f orbitals, such as Ce and Pr, may exhibit magnetism and possibly superconductivity. Sato *et al.* [24] reported that CeIr<sub>3</sub> is a type-II superconductor with a  $T_C = 3.4$  K, which is the second highest  $T_C$  amongst the Ce-based compounds. The small value of the Sommerfeld coefficient, 23 mJ K<sup>-2</sup> mole<sup>-1</sup>, indicates that CeIr<sub>3</sub> is a weakly correlated electron system [24]. The band structure and Fermi surface of LaIr<sub>3</sub> with and without spin-orbit coupling differ significantly [22], which indicates that spin-orbit coupling is expected to have a strong effect on the superconducting properties of LaIr<sub>3</sub>. The role of spin-orbit coupling is further confirmed by the evidence that  $T_C$  is lower in the isostructural LaRh<sub>3</sub> compound [25], where the spin-orbit coupling is negligible. LaIr<sub>3</sub> is thus a rare example of a lanthanide superconductor with strong spin-orbit coupling arising from the Ir-5d electrons.

In this paper, we examine the superconducting features of LaIr<sub>3</sub> using susceptibility, resistivity, heat capacity, and zero-field (ZF) and transverse-field (TF) muon spin relaxation and rotation ( $\mu$ SR) measurements. The TF- $\mu$ SR measurements suggest an isotropic  $s$ -wave

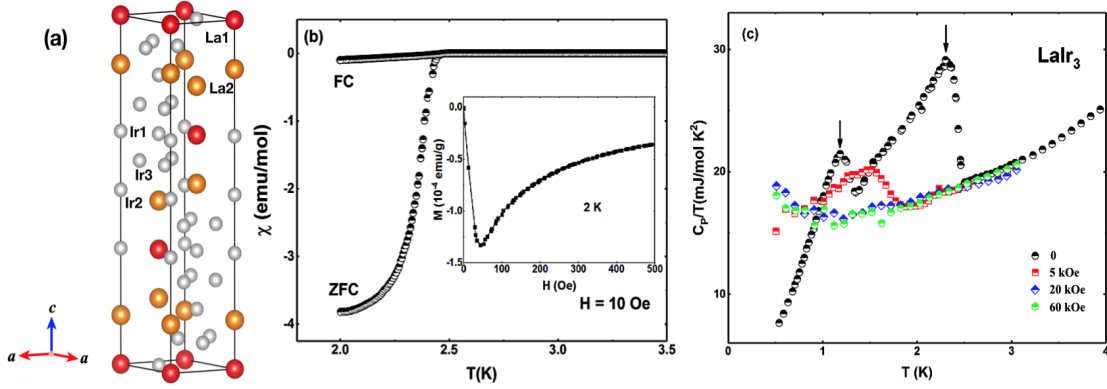


**Figure 1.** (a) Crystal structure of rhombohedral  $\text{LaIr}_3$ . The red spheres represent La1 atoms, yellow spheres are La2 atoms, and the small grey spheres represent the Ir atoms (Ir1, Ir2, and Ir3). (b) Susceptibility as a function of temperature of  $\text{LaIr}_3$  with  $H = 10$  Oe collected using ZFC and FC protocols. Inset of (b) shows the isothermal field dependence of the magnetization at 2 K. (c)  $C_P/T$  vs  $T$  in different applied magnetic fields.

model can describe the superconducting ground state of  $\text{LaIr}_3$ . The ZF- $\mu$ SR data show no evidence for internal magnetic fields below  $T_C$ , implying time-reversal symmetry is preserved for  $\text{LaIr}_3$ .

## 2. Experimental Details

Polycrystalline samples of  $\text{LaIr}_3$  were prepared by arc melting the constituent elements using a tri-arc furnace. The crystal structure was determined by powder X-ray diffraction utilizing a Panalytical X-Pert Pro diffractometer. Energy dispersive X-ray spectroscopy (EDS) in an FEI XL30 FEG-SEM system was used to investigate the stoichiometry (ratio of La:Ir) of the sample, and revealed an average chemical composition of  $\text{LaIr}_{3.1}$ , a composition with a slight excess of Ir. Zero-field-cooled (ZFC) and field-cooled (FC) DC magnetic susceptibility measurements were made using a Quantum Design (QD) Magnetic Property Measurement System, superconducting quantum interference device magnetometer. Heat capacity was measured as a function of temperature  $T$  down to 350 mK in applied magnetic fields  $H$  of up to 60 kOe using a two- $\tau$  relaxation technique in a QD Physical Property Measurement System (PPMS) with a He-3 insert. The measurements were carried out on a solid piece of a sample taken from the arc-melted button. Resistivity measurements as a function of temperature at fixed applied field and as a function of applied field at fixed temperature were made in a QD PPMS. The sample was cut into an approximately rectangular bar. Silver wires were fixed to the sample in a four-point geometry using DuPont 4929N silver paste. Measurements at higher temperature (1.8 to 3 K) in fields up to 6 kOe were made using an AC technique with an excitation current of 1 mA at a frequency of 113 Hz. Measurements at lower temperature (0.5 to 2 K) in fields up to 12 kOe were made with a He-3 insert using a pseudo-AC method, with a 400 mA DC current passed through the sample in both directions. The upper critical field was taken to be at the midpoint of the transition from the normal into the superconducting state.

$\mu$ SR measurements were performed using the MuSR spectrometer at the ISIS Neutron and

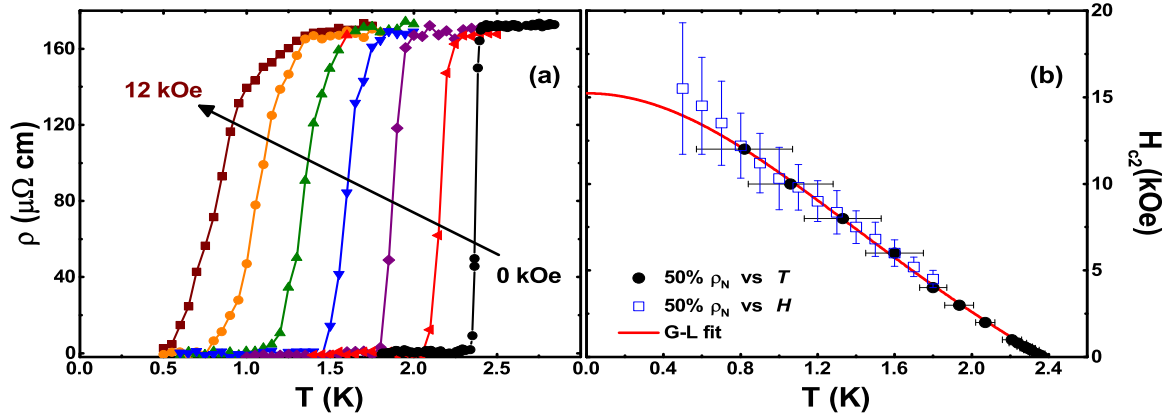


**Figure 2.** (a) Resistivity versus temperature in applied magnetic fields of 0 to 12 kOe in 2 kOe increments. (b) Upper critical field as a function of temperature, determined from  $\rho$  vs  $T$  measurements. The solid red line shows a fit using the Ginzburg-Landau (GL) model.

Muon Source, Rutherford Appleton Laboratory, United Kingdom. In the zero-field mode, the 64 detectors were placed in a longitudinal configuration and in the transverse-field mode, the spectrometer was rotated by  $90^\circ$ . The arc-melted button of  $\text{LaIr}_3$  was ground to a fine powder and mounted on a high purity (99.995%) silver plate using GE varnish. The sample could be cooled to 100 mK using a dilution refrigerator. During the ZF measurements, the magnetic field at the sample position was held at less than 10 mOe by an active compensation system. The muon beam is deposited in the sample and the muons decay, with the emitted positrons counted in detectors placed either forward or backward of the initial muon spin direction. The time dependence of the asymmetry spectra were determined using  $G_z(t) = [N_F(t) - \alpha N_B(t)] / [N_F(t) + \alpha N_B(t)]$ , where  $N_B(t)$  and  $N_F(t)$  are the number of positron counts and the constant  $\alpha$  can be calculated from a calibration measurement made in a transverse-field of 20 Oe. The ZF and TF- $\mu$ SR data were analyzed using the WiMDA software [26].

### 3. Results and Discussion

#### 3.1. Crystal structures and magnetization

Powder x-ray diffraction data confirmed the rhombohedral structure of the  $\text{LaIr}_3$  sample with the space group  $166 (R\bar{3}m)$  [22]. Fig. 1(a) shows the crystal structure of  $\text{LaIr}_3$ . The unit cell of  $\text{LaIr}_3$  contains two distinct La sites (La1 and La2) and three Ir sites (Ir1, Ir2, and Ir3). The superconductivity in  $\text{LaIr}_3$  was confirmed by the ZFC and FC susceptibility  $\chi(T)$  data, as shown in Fig. 1(b). The low-field  $\chi(T)$  data demonstrate a strong diamagnetic signal resulting from the Meissner effect below  $T_C = 2.5$  K. The magnetization  $M(H)$  curve at 2 K shown in the inset of Fig. 1(b) suggests type-II superconductivity. The lower critical field is found to be around 35 Oe at 2 K.

### 3.2. Resistivity

The temperature dependence of the electrical resistivity for LaIr<sub>3</sub> between 50 mK and 3.0 K in various applied magnetic fields is presented in Fig. 2(a). In zero field, the resistivity of LaIr<sub>3</sub> undergoes a superconducting transition at  $T_C = 2.4$  K. It is to be noted that the resistivity in the normal state just above the transition temperature of our sample is higher (by a factor of 5) than the value reported by Haldolaarachchige *et al.* [22]. This could be due to micro-cracks in our sample. As expected, the superconducting transition becomes broader and the  $T_C$  shifts to lower temperature as the applied magnetic field is increased. The resistivity data were used to extract the upper critical field  $H_{c2}$ . The  $H_{c2}(T)$  data at higher temperature and lower field can be fit using a standard Ginzburg–Landau (G-L) expression,  $H_{c2}(T) = H_{c2}(0) [(1 - t^2)/(1 + t^2)]$ , where  $t = T/T_C$  giving  $H_{c2}(0) = 15.2(1)$  kOe. This is lower than the value reported by Haldolaarachchige *et al.* [22]. Near  $T_C$ ,  $\frac{dH_{c2}}{dT} = -6.6$  kOe/K, and using the Werthamer-Helfand-Hohenberg expression  $H_{c2}(0) = -0.693 T_C \left. \frac{dH_{c2}}{dT} \right|_{T=T_C}$  gave an upper critical field,  $H_{c2}(0) = 10.9(1)$  kOe, which is also lower than the value obtained in Ref. [22]. Both the values of  $H_{c2}(0)$  are also smaller than the weak-coupling Pauli-paramagnetic limit  $H_P = 18.3T_C = 43.4$  kOe for LaIr<sub>3</sub>.

### 3.3. Heat Capacity

Fig. 1(c) shows  $C_P(T)/T$  in different applied magnetic fields. At 2.5 K, a clear anomaly is detected in  $C_P(T)/T$  (in zero-field) implying bulk superconductivity, in agreement with the  $\chi(T)$  data. In contrast to Ref. [22], the studied LaIr<sub>3</sub> sample show a very uniform transition temperature as obtained from various measurements, designating that approx. 2.4-2.5 K is the real bulk  $T_C$ . A second transition is observed in the heat capacity at 1.2 K, which is reminiscent of the second peak seen in the heat capacity of superconducting UPt<sub>3</sub> [27]. Our TF- $\mu$ SR studies do not show any signature of the lower transition and additional studies are needed in order to identify the origin of the second transition. There is no difference between the ZF- $\mu$ SR data at 0.09 and 4 K, and this supports the view that the second transition is not due to a magnetic impurity. In the presence of a 60 kOe field, the heat capacity jump is fully suppressed. The electronic and lattice heat capacity coefficients,  $\gamma$  and  $\beta$ , respectively, were calculated from the 60 kOe data, which is much higher than the upper critical field, by fitting  $C_P(T)/T = \gamma + \beta T^2$ , giving a Sommerfeld constant  $\gamma = 15.3(1)$  mJ/(mol-K<sup>2</sup>),  $\beta = 0.56(1)$  mJ/(mol-K<sup>4</sup>). Using this value of  $\beta$  ( $= nN_A \frac{12}{5} \pi^4 R \Theta_D^{-3}$ , where  $R = 8.314$  J/mol-K), gives a Debye temperature  $\Theta_D = 430(4)$  K. The estimated value of  $\gamma$  for LaIr<sub>3</sub> is very similar to that observed in CaIr<sub>2</sub> superconductor [19] and other Ir-based superconductors [17]. In the case of LaIr<sub>3</sub>, the low value of the Sommerfeld constant may be due to the lack of *f*-orbitals near the Fermi surface. Using the value of heat capacity jump at 2.5 K, the dimensionless parameter  $\Delta C_P/\gamma T_C \sim 1$  which is lower than the 1.43 expected in the BCS weak-coupling limit.

### 3.4. Superconducting gap structures

Figs. 3(a) and 3(b) present the time dependence of the TF- $\mu$ SR asymmetry spectra around  $T_C$  while Fig. 3(c) shows the corresponding maximum entropy plots. The maximum-entropy (ME) method used to analyse the TF- $\mu$ SR data is based on the Burg algorithm [28, 29] which draws on auto-regression prediction techniques. In contrast to Fourier transforms (FT), ME is useful for data collected over short-time windows and for noisy data, and does not suffer from truncation consequences, like FT sine wiggles. It provides a simultaneous interpretation

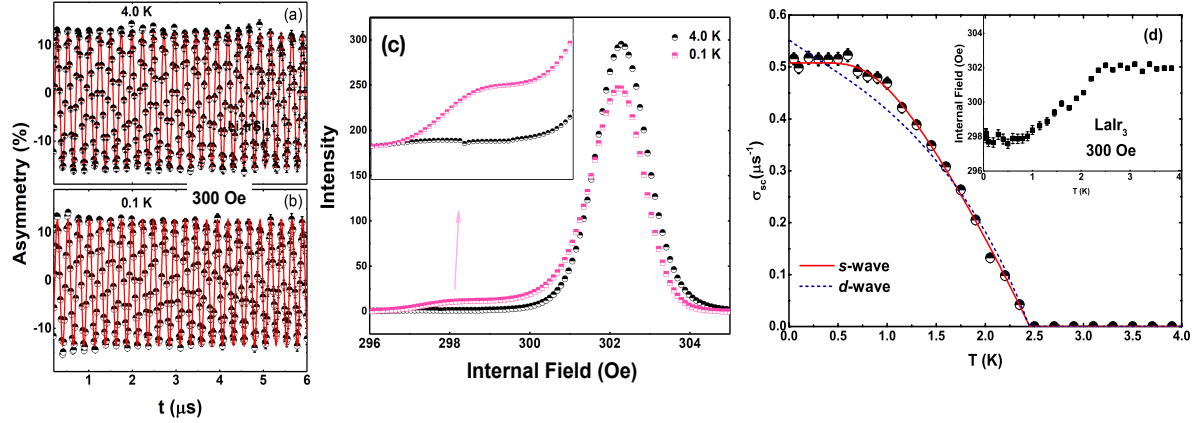


**Figure 3.** TF- $\mu$ SR spin precession signals of LaIr<sub>3</sub> taken at  $H = 300$  Oe. Time dependence asymmetry spectra (a) at 4.0 K, above  $T_C$  and (b) at 0.1 K, below  $T_C$ . The solid red lines indicate the fits to the data using Eq. 1. (c) Maximum entropy spectra (above and below  $T_C$ ). Inset of Fig. 3(c) shows the part of field distribution originating from the vortex state. (d) Temperature dependence of the depolarization rate  $\sigma_{sc}(T)$  where the solid line and dotted line are fits to the data employing an isotropic  $s$ -wave model and a  $d$ -wave model with line nodes, respectively, using Eq. 2. Inset of (d) shows the variation of the internal field with temperature.

of the asymmetry spectra from various detectors with distinct phases to produce a single frequency spectrum. At  $T \geq T_C$ , the muon depolarization is due to static nuclear moments and the resulting field distribution is centred near the applied field  $H$ . At  $T \leq T_C$ , the muon depolarization has a reasonable damping and the field distribution has two components, the first one close to the applied field  $H$  and the second shifted to a lower field value. The inset of Fig. 3(c) shows the portion of the field distribution arising from the vortex lattice. In order to investigate the superconducting order parameters and the pairing mechanism of LaIr<sub>3</sub> compound, we have carefully examined the TF- $\mu$ SR data. Below  $T_C$ , the TF asymmetry spectra which decay due to the superconducting vortex state, could be fit by an oscillatory decaying function [31, 32, 33, 34, 35],

$$G_{z1}(t) = A_1 \cos(\omega_1 t + \Phi) \exp\left(\frac{-\sigma^2 t^2}{2}\right) + A_2 \cos(\omega_2 t + \Phi), \quad (1)$$

where  $A_1$  and  $A_2$  are the transverse field asymmetries, and  $\omega_1$  and  $\omega_2$  are the frequencies that emerge from the LaIr<sub>3</sub> sample and background silver holder respectively.  $\Phi$  is the initial phase and  $\sigma$  is the total depolarization rate. The superconducting contribution  $\sigma_{sc}$  is calculated from  $\sigma_{sc} = \sqrt{\sigma^2 - \sigma_n^2}$ , where  $\sigma_n$  is the nuclear contribution which was obtained from the value of  $\sigma$  above  $T_C$ . The fitting to the lowest temperature TF data yields  $A_1 \sim 25\%$  and  $A_2 \sim 75\%$ . In the TF- $\mu$ SR fits shown in Fig. 3(d),  $A_2$  is fixed and  $A_1$  is allowed to vary. The inset of Fig. 3(d) exhibits the onset of superconductivity below  $T_C$  which is marked by a drop in the internal field. The temperature dependence of the magnetic penetration depth can be modelled using [30, 31, 34]

$$\begin{aligned} \frac{\sigma_{sc}(T)}{\sigma_{sc}(0)} &= \frac{\lambda^{-2}(T, \Delta_0)}{\lambda^{-2}(0, \Delta_0)} \\ &= 1 + \frac{1}{\pi} \int_0^{2\pi} \int_{\Delta(T)}^{\infty} \left(\frac{\delta f}{\delta E}\right) \times \frac{EdE d\phi}{\sqrt{E^2 - \Delta(T, \Delta)^2}}, \end{aligned} \quad (2)$$

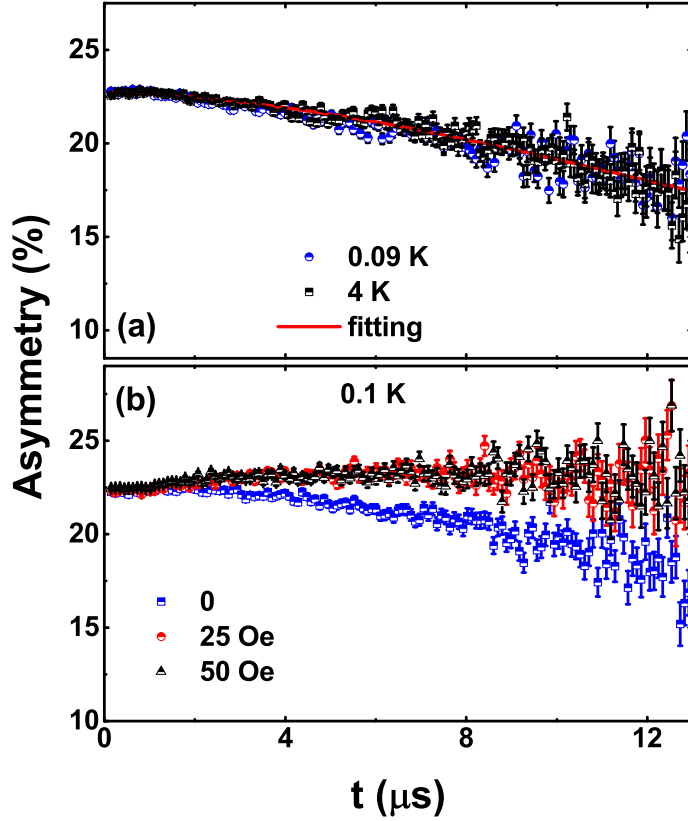


**Figure 4.** (Color online) (a) Time dependence of zero-field asymmetry spectra for  $\text{LaIr}_3$  collected at 0.09 K (circles) and 4.0 K (squares). The lines are least squares fits to the ZF data made using Eqs. (4) and (5). (b) Longitudinal field asymmetry spectra taken at 0.1 K in the presence of various applied field  $H$ .

where  $f = [1 + \exp(-E/k_B T)]^{-1}$  is the Fermi function,  $\phi$  is the angle along the Fermi surface, and  $\Delta(T, 0) = \Delta_0 \delta(T/T) g(\phi)$ . The superconducting gap was approximated using  $\delta(T/T_C) = \tanh[1.82(T_C/T - 1)]^{0.51}$  where  $g(\phi)$  gives the angular dependence of gap and  $\phi$  is the polar angle for the anisotropy.  $g(\phi)$  is replaced with (a) 1 for an isotropic  $s$ -wave gap and (b)  $|\cos(2\phi)|$  for a nodal  $d$ -wave gap [36, 37]. For  $\text{LaIr}_3$ , the  $\lambda^{-2}(T)$  data can be modelled satisfactorily by employing an isotropic  $s$ -wave gap with a value of 0.35(1) meV. The gap to  $T_C$  ratio is found to be  $2\Delta(0)/k_B T_C = 3.31(1)$ , which lower than the value 3.56 expected from BCS theory. This suggests weak-coupling superconductivity in the case of  $\text{LaIr}_3$  which is in agreement with the heat capacity data. TF- $\mu$ SR measurements of  $\text{Mg}_{10}\text{Ir}_{19}\text{B}_{16}$  reveal spin-singlet  $s$ -wave pairing, even though the lack of inversion symmetry and large SO coupling of  $\text{Mg}_{10}\text{Ir}_{19}\text{B}_{16}$  should produce a mixed pairing state, likely with a large spin-triplet contribution [38]. TF- $\mu$ SR data on  $\text{La}_7\text{Ir}_3$  compound also reveal a gap with an isotropic  $s$ -wave pairing symmetry [39].

The muon depolarization rate below  $T_C$  is linked to the magnetic penetration depth,  $\lambda$ . In case of a triangular [40, 41, 42] lattice  $\frac{\sigma_{sc}^2}{\gamma_\mu^2} = \frac{0.00371 \times \phi_0^2}{\lambda^4}$ , where  $\phi_0 = 2.07 \times 10^{-15} \text{ Tm}^2$ , is the flux quantum number and  $\gamma_\mu/2\pi = 135.5 \text{ MHz T}^{-1}$ , is the muon gyromagnetic ratio. From the  $s$ -wave fit, we estimate that the magnetic penetration depth  $\lambda(0) = 386(3) \text{ nm}$ . London's theory [40] gives the relation between  $\lambda$  ( $= \lambda_L$ ) and other microscopic parameters

such as  $\lambda_L^2 = \frac{m^*c^2}{4\pi n_s e^2}$ , where  $m^* = (1 + \lambda_{e-ph})m_e$  is the effective mass and  $n_s$  is the density of superconducting carriers, and hence one can calculate  $m^*$  and  $n_s$ . The electron-phonon coupling constant  $\lambda_{e-ph}$  can be calculated using the Debye temperature,  $\Theta_D$ , and  $T_C$  using McMillan's relation which is also valid in the weak-coupling limit [43, 44].

$$\lambda_{e-ph} = \frac{1.04 + \mu^* \ln(\Theta_D/1.45T_C)}{(1 - 0.62\mu^*) \ln(\Theta_D/1.45T_C) - 1.04}, \quad (3)$$

where  $\mu^*$  is the Coulomb pseudo-potential. McMillan states [43] that  $\mu^* = 0.1$  is confirmed for the nearly-free electrons metals such as zinc, and  $\mu^* = 0.15$  is reasonable for most of the intermetallic superconductors [44, 45, 46, 47]. Furthermore, P. B. Allen [44] has stated that for conventional metals  $\mu^* \leq 0.2$ . Using  $\mu^* = 0.15$  [22], we find  $\lambda_{e-ph} = 0.53$ . Using the estimated value of  $\lambda_{e-ph}$  and  $\lambda_L(0)$ , the superconducting carrier density is estimated to be  $n_s = 2.9(1) \times 10^{27}$  carriers  $m^{-3}$  and the effective-mass enhancement  $m^* = 1.53m_e$  for LaIr<sub>3</sub>.

### 3.5. Zero-field muon spin relaxation

Fig. 4(a) shows the time dependence of ZF asymmetry spectra from LaIr<sub>3</sub> at  $T \geq T_C$  and  $T \leq T_C$ . At  $T \leq T_C$ , there is no change of muon asymmetry spectra compared to the spectra collected at  $T \geq T_C$ , which suggests that time-reversal symmetry is preserved in LaIr<sub>3</sub>. The ZF data for LaIr<sub>3</sub> can be modelled using the damped Kubo-Toyabe (KT) function [48, 49, 50, 51],

$$G_{z2}(t) = A_0 G_{KT}(t) e^{-\lambda t} + A_{bg}, \quad (4)$$

where

$$G_{KT}(t) = \left[ \frac{1}{3} + \frac{2}{3} (1 - \sigma_{KT}^2 t^2) e^{-\frac{\sigma_{KT}^2 t^2}{2}} \right] \quad (5)$$

the Kubo-Toyabe function, models the change in asymmetry arising from static nuclear moments and  $\lambda$ ,  $A_0$ , and  $A_{bg}$  are the electronic relaxation rate, initial sample asymmetry, and background asymmetry, respectively. The fits to the ZF data using Eqs. 4 and 5 give  $\sigma_{KT} = 0.041(5) \mu s^{-1}$  and  $\lambda = 0.018(3) \mu s^{-1}$  at 0.09 K and  $\sigma_{KT} = 0.041(1) \mu s^{-1}$  and  $\lambda = 0.013(2) \mu s^{-1}$  at 4 K, while the fit parameters  $A_0$  and  $A_{bg}$  are found to be temperature independent. Furthermore, the ZF- $\mu$ SR spectra measured in longitudinal fields of 25 and 50 Oe at 0.1 K (Fig. 4(b)) revealed the decoupling of the muon spins from the static nuclear fields at the muon stopping sites.

Our ZF- $\mu$ SR measurements indicate time-reversal symmetry is preserved in LaIr<sub>3</sub>. A similar result is found in the Ir-based superconductor In Mg<sub>10</sub>Ir<sub>19</sub>B<sub>16</sub> [38], while in the case of La<sub>7</sub>Ir<sub>3</sub>, ZF- $\mu$ SR data confirm that the superconducting ground state breaks time-reversal symmetry [39].

## 4. Summary

In summary, we have examined the superconducting gap structure and pairing symmetry of LaIr<sub>3</sub> using TF and ZF- $\mu$ SR measurements. Bulk type-II superconductivity is observed in the susceptibility measurements with  $T_C = 2.5(1)$  K. Similar to UPt<sub>3</sub>, two transitions are seen in the heat capacity data and the origin of the lower temperature feature remains unclear at this time. Transverse field- $\mu$ SR measurements reveal a fully gapped *s*-wave type superconductivity

with the gap to  $T_C$  ratio,  $2\Delta(0)/k_B T_C = 3.31$ , compared to 3.56 (BCS value) suggesting weak-coupling superconductivity. Our ZF- $\mu$ SR data do not reveal any sign of internal fields below  $T_C$ , which indicates that time reversal symmetry is preserved in  $\text{LaIr}_3$ . The results underline the need for further research into the properties of Ir-based intermetallic superconductors and especially those that have a noncentrosymmetric structure, where strong antisymmetric spin-orbit coupling could lead to unconventional superconductivity, perhaps with a mixed spin singlet-triplet pairing.

### Acknowledgments

AB would like to acknowledge DST India, for an Inspire Faculty Research Grant (DST/INSPIRE/04/2015/000169). DTA and ADH would like to thank CMPC-STFC, grant number CMPC-09108, and also DIST for financial support. DTA thanks the Japan Society for the Promotion of Science (JSPS) for an Invitational Fellowship.

### References

- [1] Kim J B, Jin H, Moon S J, Kim J -Y, Park B -G, Leem C S, Yu J, Noh T W, Kim C, Oh S -J, Park J -H, Durairaj V, Cao G and Rotenberg E 2008 Novel  $J_{\text{eff}}=1/2$  Mott State Induced by Relativistic Spin-Orbit Coupling in  $\text{Sr}_2\text{IrO}_4$  *Phys. Rev. Lett.* **101**, 076402
- [2] Kim B J, Ohsumi H, Komesu T, Sakai S, Morita T, Takagi H and Arima T 2009 Phase-Sensitive Observation of a Spin-Orbital Mott State in  $\text{Sr}_2\text{IrO}_4$  *Science* **323**, 1329
- [3] Moon S J, Jin H, Kim K W, Choi W S, Lee Y S, Yu J, Cao G, Sumi A, Funakubo H, Bernhard C and Noh T W 2008 Dimensionality-Controlled Insulator-Metal Transition and Correlated Metallic State in 5d Transition Metal Oxides  $\text{Sr}_{n+1}\text{Ir}_n\text{O}_{3n+1}$  ( $n=1, 2$ , and  $\infty$ ) *Phys. Rev. Lett.* **101**, 226402
- [4] Hirai D, Takayama T, Hashizume D, Higashinaka R, Yamamoto A, Hiroko A K and Takag H 2010 Superconductivity in 4d and 5d transition metal layered pnictides  $\text{BaRh}_2\text{P}_2$ ,  $\text{BaIr}_2\text{P}_2$  and  $\text{SrIr}_2\text{As}_2$  *Physica C* **470**, S296
- [5] Kim J H, Casa D, Upton M H, Gog T, Kim Y -J, Mitchell J F, Veenendaal M van, Daghofer M, van den Brink J, Khaliullin G and Kim B J 2012 Magnetic Excitation Spectra of  $\text{Sr}_2\text{IrO}_4$  Probed by Resonant Inelastic X-Ray Scattering: Establishing Links to Cuprate Superconductors *Phys. Rev. Lett.* **108**, 177003
- [6] Jackeli G and Khaliullin G 2009 Mott Insulators in the Strong Spin-Orbit Coupling Limit: From Heisenberg to a Quantum Compass and Kitaev Models *Phys. Rev. Lett.* **102**, 017205
- [7] Singh Y, Manni S, Reuther J, Berlijn T, Thomale R, Ku W, Trebst S and Gegenwart P 2012 Relevance of the Heisenberg-Kitaev Model for the Honeycomb Lattice Iridates  $\text{A}_2\text{IrO}_3$  *Phys. Rev. Lett.* **108**, 127203
- [8] Choi S K, Coldea R, Kolmogorov A N, Lancaster T, Mazin I I, Blundell S J, Radaelli P G, Singh Y, Gegenwart P, Choi K R, Cheong S -W, Baker P J, Stock C and Taylor J 2012 Spin Waves and Revised Crystal Structure of Honeycomb Iridate  $\text{Na}_2\text{IrO}_3$  *Phys. Rev. Lett.* **108**, 127204
- [9] Sipoš B, Kusmartseva A F, Akrap A, Berger H, Forro L and Tutiš E 2008 From Mott state to superconductivity in 1T-TaS<sub>2</sub> *Nat. Mater.* **7**, 960
- [10] Bauer E, Hilscher G, Michor H, Paul Ch, Scheidt E W, Griбанov A, Seropegin Yu, Noel H, Sigrist M and Rogl P 2004 Heavy Fermion Superconductivity and Magnetic Order in Noncentrosymmetric  $\text{CePt}_3\text{Si}$  *Phys. Rev. Lett.* **92**, 027003
- [11] Hanawa N, Muraoka Y, Tayama T, Sakakibara T, Yamaura J and Hiroi Z 2001 Superconductivity at 1 K in  $\text{Cd}_2\text{Re}_2\text{O}_7$  *Phys. Rev. Lett.* **87**, 187001
- [12] Yonezawa S, Muraoka Y, Matsushita Y, and Hiroi Z 2004 Superconductivity in a pyrochlore-related oxide  $\text{KOs}_2\text{O}_6$  *J. Phys.: Condens. Matter* **16**, L9-L12

- [13] Guo J G, Qi Y P, Matsuishi S and Hosono H 2012 Tc Maximum in Solid Solution of Pyrite IrSe<sub>2</sub>RhSe<sub>2</sub> Induced by Destabilization of Anion Dimers *J. Am. Chem. Soc.* **134**, 20001
- [14] Suzuki H, Furubayashi T, Cao G H, Kitazawa H, Kamimura A, Hirata K and Matsumoto T 1999 Metal-insulator transition and superconductivity in spinel-type system Cu<sub>1-x</sub>Zn<sub>x</sub>Ir<sub>2</sub>S<sub>4</sub> *J. Phys. Soc. Japan* **68**, 2495
- [15] Sugitani I, Okuda Y, Shishido H, Yamada T, Thamizhavel A, Yamamoto E, Matsuda T D, Haga Y, Takeuchi T, Settai R and Onuki Y 2006 Pressure-Induced Heavy-Fermion Superconductivity in Antiferromagnet CeIrSi<sub>3</sub> without Inversion Symmetry *J. Phys. Soc. Japan* **75**, 043703
- [16] Okamoto Y, Inohara T, Yamakawa Y, Yamakage A and Takenaka K 2016 Superconductivity in the hexagonal ternary phosphide ScIrP *J. Phys. Soc. Japan* **85**, 013704
- [17] Qi Y P, Guo J G, Lei J C, Xiao Z W, Kamiya T and Hosono H 2014 Superconductivity in noncentrosymmetric ternary equiatomic pnictides LaMP ( = Ir and Rh; P = P and As) *Phys. Rev. B* **89**, 024517
- [18] Berry N, Capan C, Seyfarth G, Bianchi A D, Ziller J and Fisk Z 2009 Superconductivity without Fe or Ni in the phosphides BaIr<sub>2</sub>P<sub>2</sub> and BaRh<sub>2</sub>P<sub>2</sub> *Phys. Rev. B* **79**, 180502(R)
- [19] Tutuncu H M, Uzunok H Y, Karaca E, Arslan E and Srivastava G P 2017 Effects of spin-orbit coupling on the electron-phonon superconductivity in the cubic Laves-phase compounds CaIr<sub>2</sub> and CaRh<sub>2</sub> *Phys. Rev. B* **96**, 134514
- [20] Hirai D, Ali M N and Cava R J 2013 Strong electron-phonon coupling superconductivity induced by a low-lying phonon in IrGe *J. Phys. Soc. Jpn.* **82**, 124701
- [21] Klimczuk T, Ronning F, Sidorov V, Cava R J and Thompson J D 2007 Physical Properties of the Noncentrosymmetric Superconductor Mg<sub>10</sub>Ir<sub>19</sub>B<sub>16</sub> *Phys. Rev. Lett.* **99**, 257004
- [22] Haldolaarachchige N, Schoop L, Khan M A, Huang W, Ji H, Hettiarachchilage K and Young D P 2017 Ir *d*-band derived superconductivity in the lanthanum-iridium system LaIr<sub>3</sub> *J. Phys.: Condens. Matter* **29**, 475602
- [23] Huber J G 1990 Probing *d*-band superconductivity in XIr<sub>3</sub> compounds *Physica* **163**, 219-223
- [24] Sato Y J, Nakamura A, Shimizu Y, Maurya A, Homma Y, Li D, Honda F and D. Aoki 2018 Superconducting Properties of CeIr<sub>3</sub> Single Crystal *J. Phys. Soc. Jpn.* **87**, 053704
- [25] Geballe T H, Matthias B T, Compton V B, Corenzwit E, Hull G W and Longinotti D 1965 *Phys. Rev.* **137**, A119
- [26] Pratt F L 2000 WIMDA: a muon data analysis program for the Windows PC *Physica B* **289-290**, 710
- [27] Trappmann T and Lohneysen H v and Taillefer L 1991 Pressure dependence of the superconducting phases in UPt<sub>3</sub> *Phys. Rev. B* **43**, 13714
- [28] Jones J A, and P J Hore 1991 The maximum entropy method. Appearance and reality *Journal of Magnetic Resonance* (1969) **92**, 363-376; Stephenson D S 1988 Linear prediction and maximum entropy methods in NMR spectroscopy *Progress in NMR Spectroscopy* **20**, 515
- [29] Rainford B D, and Daniell G J 1994  $\mu$ SR frequency spectra using the maximum entropy method *Hyperfine Interactions* **87**, 1129
- [30] Bhattacharyya A, Adroja D T, Panda K, Saha S, Das T, Machado A J S, Cigarroa O V, Grant T W, Fisk Z, Hillier A D and Manfrinetti P 2019 Evidence of a Nodal Line in the Superconducting Gap Symmetry of Noncentrosymmetric ThCoC<sub>2</sub> *Phys. Rev. Lett.* **122**, 147001
- [31] Bhattacharyya A, Adroja D T, Quintanilla J, Hillier A D, Kase N, Strydom A M and Akimitsu J 2015 Broken time-reversal symmetry probed by muon spin relaxation in the caged type superconductor Lu<sub>5</sub>Rh<sub>6</sub>Sn<sub>18</sub> *Phys. Rev. B* **91**, 060503(R)
- [32] Bhattacharyya A, Adroja D T, Kase N, Hillier A D, Akimitsu J and Strydom A M 2015 Unconventional superconductivity in Y<sub>5</sub>Rh<sub>6</sub>Sn<sub>18</sub> probed by muon spin relaxation *Sci. Rep.* **5**, 12926
- [33] Bhattacharyya A, Adroja D T, Kase N, Hillier A D, Strydom A M and Akimitsu J 2018 Unconventional superconductivity in the cage-type compound Sc<sub>5</sub>Rh<sub>6</sub>Sn<sub>18</sub>. *Physical Review B.* **98** 024511

- [34] Adroja D T, Bhattacharyya A, Telling M, Feng Y, Smidman M, Pan B, Zhao J, Hillier A D, Pratt F L and Strydom A M 2015 Superconducting ground state of quasi-one-dimensional  $K_2Cr_3As_3$  investigated using  $\mu$ SR measurements *Phys. Rev. B* **92**, 134505
- [35] Bhattacharyya A, Adroja D T, Smidman M and Anand V K 2018 A brief review on  $\mu$ SR studies of unconventional Fe- and Cr-based superconductors *Sci. China-Phys. Mech. Astron.* **61**, 127402
- [36] Annett J F 1990 Symmetry of the order parameter for high-temperature superconductivity *Adv. Phys.* **39**, 83
- [37] Pang G M, Smidman M, Jiang W B, Bao J K, Weng Z F, Wang Y F, Jiao L, Zhang J L, Cao G H and Yuan H Q 2015 Evidence for nodal superconductivity in quasi-one-dimensional  $K_2Cr_3As_3$  *Phys. Rev. B* **91**, 220502(R)
- [38] Aczel A A, Williams T J, Goko T, Carlo J P, Yu W, Uemura Y J, Klimczuk T, Thompson J D, Cava R J and Luke G M 2010 Muon spin rotation/relaxation measurements of the noncentrosymmetric superconductor  $Mg_{10}Ir_{19}B_{16}$  *Phys. Rev. B* **82**, 024520
- [39] Barker J A T, Singh D, Thamizhavel A, Hillier A D, Lees M R, Balakrishnan G, Paul D McK and Singh R P 2015 Unconventional Superconductivity in  $La_7Ir_3$  Revealed by Muon Spin Relaxation: Introducing a New Family of Noncentrosymmetric Superconductor That Breaks Time-Reversal Symmetry *Phys. Rev. Lett.* **115**, 267001
- [40] Sonier J E, Brewer J H and Kiefl R F 2000  $\mu$ SR studies of the vortex state in type-II superconductors *Rev. Mod. Phys.* **72**, 769
- [41] Chia E E M, Salamon M B, Sugawara H and Sato H 2004 Probing the superconducting gap symmetry of  $PrRu_4Sb_{12}$ : A comparison with  $PrOs_4Sb_{12}$  *Phys. Rev. B* **69**, 180509(R)
- [42] Amato A 1997 Heavy-fermion systems studied by  $\mu$ SR technique *Rev. Mod. Phys.* **69**, 1119
- [43] McMillan W L 1968 Transition temperature of strong-coupled superconductors *Phys. Rev.* **167**, 331
- [44] Allen P B, 1999 Handbook of Superconductivity, edited by C. P. Poole Academic Press, New York : Chp 9 478.
- [45] Verchenko V Y, Tsirlin A A, Zbtsovskiy A O and Shevelkov A V 2016 Strong electron-phonon coupling in the intermetallic superconductor  $Mo_8Ga_41$  *Phys. Rev. B* **93**, 064501
- [46] Singh D, Hillier A D, Thamizhavel A and Singh R P 2016 Superconducting properties of the noncentrosymmetric superconductor  $Re_6Hf$  *Phys. Rev. B* **94**, 054515
- [47] Carnicom E M et al 2018  $TaRh_2B_2$  and  $NbRh_2B_2$ : superconductors with a chiral noncentrosymmetric crystal structure *Sci. Adv.* **4**, eaar7969
- [48] Adroja D T, Bhattacharyya A, Biswas P K, Smidman M, Hillier A D, Mao H, Luo H, Cao G -H, Wang Z and Wang C 2017 Multigap superconductivity in  $ThAsFeN$  investigated using  $\mu$ SR measurements *Phys. Rev. B* **96**, 144502
- [49] Adroja D T, Bhattacharyya A, Telling M, Feng Y, Smidman M, Pan B, Zhao J, Hillier A D, Pratt F L and Strydom A M 2015 Superconducting ground state of quasi-one-dimensional  $K_2Cr_3As_3$  investigated using  $\mu$ SR measurements *Phys. Rev. B* **92**, 134505
- [50] Adroja D T, Bhattacharyya A, Smidman M, Hillier A D, Feng Y, Pan B, Zhao J, Lees M R, Strydom A M and Biswas P K 2017 Nodal Superconducting Gap Structure in the Quasi-One-Dimensional  $Cs_2Cr_3As_3$  Investigated Using  $\mu$ SR Measurements *J. Phys. Soc. Jpn.* **86**, 044710
- [51] Bhattacharyya A, Adroja D T, Hillier A D, Jha R, Awana V P S and Strydom A M 2017 Superconducting gap structure in the electron doped  $BiS_2$ -based superconductor *J. Phys.: Condens. Matter* **29**, 265602